Gold(I) N-heterocyclic Carbene Complexes with 7-Azaindoles Demonstrate *In Vitro* Antiproliferative Effects on Ovarian Cancer Cells and Anti-inflammatory Activity

Zdeněk Trávníček [*] , Ján Vančo , Jan Belza , Michal Čajan , Jan Hošek , Zdeněk Dvořák

Posted Date: 4 January 2024

doi: 10.20944/preprints202401.0375.v1

Keywords: gold(I) complex; 7-azaindoles; anticancer; anti-inflammatory; cell cycle; apoptosis.; TNF-alpha; NF-kappaB

Article

Gold(I) *N*-Heterocyclic Carbene Complexes with 7-Azaindoles Demonstrate *In Vitro* Antiproliferative Effects on Ovarian Cancer Cells and Anti-Inflammatory Activity

Zdeněk Trávníček [1,*], Ján Vančo [1], Jan Belza [1], Michal Čajan, [1] Jan Hošek [1] and Zdeněk Dvořák [2]

[1] Czech Advanced Technology and Research Institute, Regional Centre of Advanced Technologies and Materials, Palacký University, Šlechtitelů 27, CZ-779 00 Olomouc, Czech Republic; zdenek.travnicek@upol.cz; jan.vanco@upol.cz; jan.belza01@upol.cz; michal.cajan@upol.cz; jan.hosek@upol.cz

[2] Department of Cell Biology and Genetics, Faculty of Science, Palacký University, Šlechtitelů 27, CZ-779 00 Olomouc, Czech Republic; zdenek.dvorak@upol.cz

* Correspondence: zdenek.travnicek@upol.cz

Abstract: The gold(I) *N*-heterocyclic carbene (NHC) complexes, containing a combination of 1,3-bis(2,6-diisopropylphenyl)imidazol-2-ylidene (iPr) and the corresponding 7-azaindole derivative (HL1-4), were prepared and structurally characterized. The complexes of the composition of [Au(iPr)(HL*n*)], where *n* = 1–4 for 5-fluoro-7-azaindole (**1**), 5-bromo-7-azaindole (**2**), 3-chloro-7-azaindole (**3**) and 3-iodo-7-azaindole (**4**), were further evaluated for their *in vitro* anti-cancer and anti-inflammatory activities. The results showed that complexes (**1–4**) behave as considerably cytotoxic against human ovarian cancer cell line A2780 (with $IC_{50} \approx 4–9$ μM) and cisplatin-resistant cell line A2780R (with $IC_{50} \approx 5–8$ μM, except for **2** with $IC_{50} > 25$ μM), providing significantly higher cytotoxicity than anticancer drug *cisplatin*. Moreover, they also revealed a relatively good selectivity over normal cells (MRC-5), with the values of selectivity index, SI > 2.5. The complex **4** was further studied for its cellular effects in A2780 cells by cell cycle analysis, induction of apoptosis, intracellular ROS production, activation of caspases 3/7 and disruption of mitochondrial membrane potential. The ability of complexes (**1–4**) to influence the activity of pro-inflammatory transcription factor NF-κB and secretion of TNF-α were evaluated, showing that complex **4** reveals comparable effects as the inflammatory drug *Auranofin*.

Keywords: gold(I) complex; 7-azaindoles; anticancer; anti-inflammatory; TNF-α; NF-κB; cell cycle; apoptosis

1. Introduction

Gold(I) complexes containing *N*-heterocyclic carbene (NHC) ligands have attracted attention owing to their potential application in the fields of catalysis [1,2]. Thus, the chemistry of "gold(I/III)–NHC" systems has been intensively developed through the last few decades as can be documented by many publication outputs found at databases such as Web of Science (www.isiknowledge.com) and SCOPUS (www.scopus.com) utilizing a combination of suitable keywords. The most recent papers and reviews on the latter topic can be found in the literature [3–13]. The interest in gold(I)-complexes is also associated with the worldwide success of gold-based metallodrug *Auranofin* [3,4,5-triacetyloxy-6-(acetyloxymethyl)-oxane-2-thiolate-triethylphosphine)-gold(I)] complex (ATC code M01CB03; CAS: 34031-32-8) utilizable in treating rheumatoid arthritis [14–16], see Scheme 1. The references related to the above-mentioned papers may further support scientists' attraction to this topic.

In our recent work [17], we have prepared a series of *N*-heterocyclic carbene (NHC) gold(I) complexes involving 1,3-bis(2,6-diisopropylphenyl)imidazol-2-ylidene (iPr) ligand in combination

 doi:10.20944/preprints202401.0375.v1

with 6-mercaptopurine derivatives (HPur), with the general composition of [Au(iPr)(Pur)]. The complexes revealed significant *in vitro* cytotoxicity, with the best IC_{50} values of 3.4–6.4 μM against A2780 and reasonable selectivity; however, on the other side they showed only negligible effects on the production of inflammatory-related cytokine (TNF-α), the activation of nuclear factor kappa-light-chain-enhancer of activated B cells (NF-κB) and peroxisome proliferator-activated receptor gamma (PPARγ). This finding motivated us to slightly modify the composition of the mentioned complexes, and thus, we decided to prepare gold(I) complexes in which 6-mercaptopurine derivatives are replaced with 7-azaindole (HL) derivatives. The choice of these organic molecules is associated with our previous findings that Ir and Pt complexes containing these ligands showed remarkable *in vitro* cytotoxicity against various human cancer cells [18,19]. The possible utilization of the herein-reported gold(I) with 7-azaindole derivatives has already been certified by the Industrial Property Office of the Czech Republic, when the national patent CZ 307954 (titled: *N-heterocyclic carbene complexes of gold with bicyclic N-donor ligands and using these complexes to prepare antitumor therapy medicaments* has been granted [20].

In the present work, we strived to find how the utilization of selected 7-azaindole derivatives will impact on *in vitro* anticancer and anti-inflammatory activities of the final complexes of the composition [Au(iPr)(HL*n*)] (**1**–**4**).

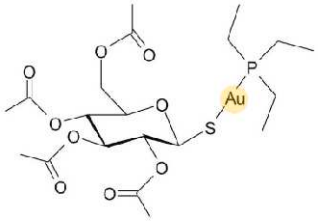

Scheme 1. The structural formula of gold(I) drug *Auranofin*.

2. Results and Discussion

2.1. Preparation and general characterization

The synthetic pathway leading to preparation of the presented complexes (**1**–**4**) of the general composition of [Au(iPr)(HL*n*)] is shown in Scheme 2. The purity and empirical formula of the corresponding complex have been deduced based on the results of CHN elemental analyses, whilst the confirmation of sum formulas can be associated with the molecular peaks observed in the mass spectra measured in MeOH in the positive mode at *m*/*z* = 783.28 (for **2**), 737.34 (for **3**) and 829.25 (for **4**) or in the negative mode at *m*/*z* = 719.34 (for **1**), see Figures S1–S4 in Supplementary materials. The complexes were further analysed using infrared spectroscopy, showing typical peaks associated with the presence of iPr and 7-azaindole moieties. The spectra are shown in Figures S5–S8 in Supplementary Materials (together with IR spectra of free ligands HL1-4 and starting [Au(iPr)Cl] complex for comparative and interpretative purposes, see Figures S9–S13), and they revealed peaks at ca 3150-3030, 2980-2860 cm^{-1} attributable to the stretching vibrations of $\nu(C–H)_{aromatic}$, and $\nu(C–H)_{aliphatic}$, respectively. The high intensity peaks at ca 1590-1540 cm^{-1} and ca 1470-1450 are assignable to $\nu(C–N)_{ring}$, and to $\nu(C–C)_{ring}$ vibrations, respectively. The coordination of the 7-azaindole moiety to gold(I) through the N1 atom can be associated with the intensive peaks at ca 450-517 cm^{-1} belonging to ν(Au–N) [21].

Preprints (www.preprints.org) | NOT PEER-REVIEWED | Posted: 4 January 2024 doi:10.20944/preprints202401.0375.v1

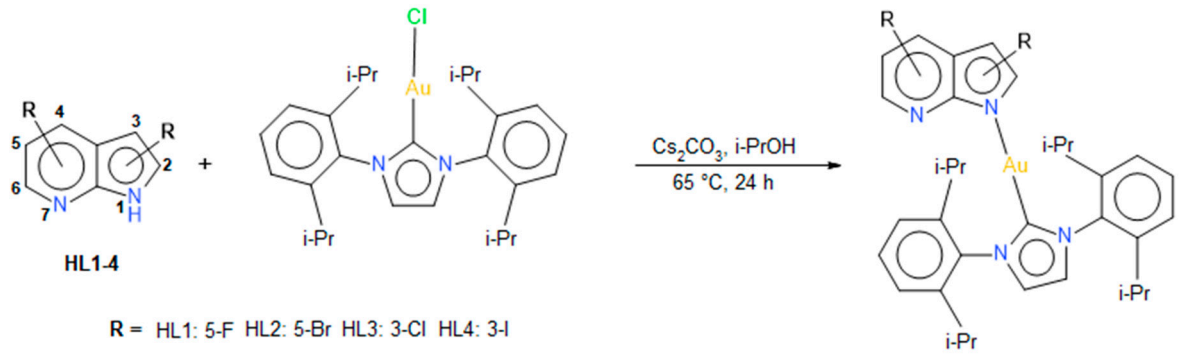

Scheme 2. The reaction pathway leading to the preparation of the presented complexes (**1**–**4**) of the general composition of [Au(iPr)(HL*n*)] together with the atoms numbering of the 7-azaindole moiety.

2.2. Single crystal X-ray analysis

The molecular structures of complexes **1** and **4** were determined using a single-crystal X-ray analysis. In each complex, the gold(I) atom is coordinated in a slightly distorted linear arrangement by the N1 atom from the 7-azaindole moiety and the C1 atoms from the imidazole ring of the NHC ligand (iPr), as can be seen from Figure 1 and Table 1. The data given in Table 1 shows, that the Au–N and Au–C bond distances are very close not only in the case of complexes **1** and **4**, but also quite comparable with those determined for similar Au(I)-NHC complexes with 6-mercaptopurine derivatives [17]. On the other side, the N–Au–C bond angles differ significantly within each of the groups, but it can be taken as a logical consequence associated with a different degree of substitution of the corresponding *N*-donor ligand together with the concrete non-covalent intra/intermolecular bonding. As for complex **1**, the individual molecules are connected through C–H···N, C–H···C hydrogen bonds into infinite 1D-polymeric chains (see Figure S14 in Supplementary Materials), while the molecules of complex **4** form non-covalent centrosymmetric dimmer connected *via* the same types of non-covalent bonds (see Figure S15 in Supplementary Materials). These non-covalent interactions further stabilize crystal packing in both structures.

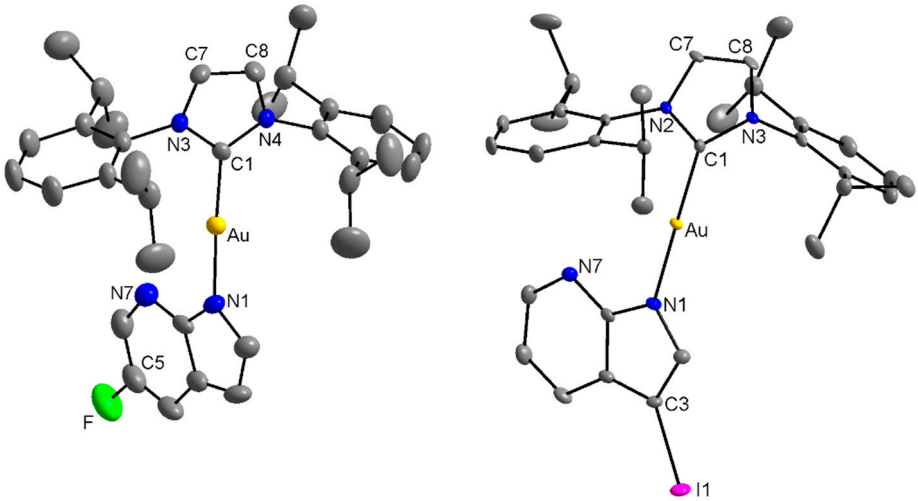

Figure 1. X-ray structures of [Au(iPr)(L1)] (**1**) *left* and [Au(iPr)(L4)] (**4**) *right*. The H-atoms, together with labelling of some carbons (dark grey) and hydrogens (light grey), are omitted for better clarity. The molecular graphics was generated using Diamond software (Crystal Impact, Bonn, Germany).

Preprints (www.preprints.org) | NOT PEER-REVIEWED | Posted: 4 January 2024 doi:10.20944/preprints202401.0375.v1

Table 1. Selected bond lengths [Å] and angles [°] [Au(iPr)(L1)] (**1**) *left* and [Au(iPr)(L4)] (**4**) and their comparison with those in similar Au(I)-NHC complexes containing the iPr moiety and 6-mercaptopurine derivatives as *N*-donor ligands.

Compound		[Au(iPr)(L1)] 1	[Au(iPr)(L4)] 4	[Au(iPr)(Pur1)]*	[Au(iPr)(Pur2)]**
Selected bond lengths [Å]	Au-N	2.026(4)	2.024(2)	2.018(3)	2.033(6)
	Au-C	1.963(5)	1.976(3)	1.974(4)	1.978(7)
Selected angle [°]	N-Au-C	175.54(18)	179.29(12)	173.58(16)	175.7(3)

* HPur1 = 6-{[(3-fluorophenyl)methyl]sulfanyl}purine. **Hpur2 = 6-{[(3-trifluoromethylphenyl)-methyl]sulfanyl}purine. The data adopted from ref. [17].

2.3. In vitro cytotoxicity studies

The *in vitro* cytotoxicity of complexes **1–4**, together with [Au(iPr)Cl], *Auranofin* and *Cisplatin* for comparative purposes, was determined against ovarian A2780 and A2780R cisplatin-resistant human cancer cell lines. The results, given in Table 2, revealed considerable *in vitro* anti-cancer effect of the complexes **1–4** on A2780, significantly exceeding cytotoxicity of both the starting [Au(iPr)Cl] complex and cytostatic drug *Cisplatin*, even though showing slightly lower activity than *Auranofin*. A very similar situation can be described in the case of A2780R cisplatin-resistant cell line, except for complex **2**, having IC_{50} > 25 μM. The more detailed analysis of cytotoxicity data obtained on both the cancer cells helped us to reveal resistance factor (RF), defined as the ratio between the IC_{50} value of the resistant cell and sensitive one IC_{50}(A2780R)/IC_{50}(A2780), and pointed out complexes **1** as highly effective against A2780R, followed by complex **4**. On the other side, the best selectivity index (SI), expressed as IC_{50}(MRC-5)/IC_{50}(A2780), showing prevailing toxicity on cancer over normal (MRC-5) cells, was found for complex **4**. For that reason, complex **4** was chosen as the representative candidate for consequent deeper analysis of its cellular effects in the A2780 cells. These results represent a significant contribution to the knowledge regarding the compounds effective against ovarian cancer. According to WHO Mortality Database (https://platform.who.int/mortality/themes/theme-details/topics/indicator-groups/indicator-group-details/MDB/ovary-cancer), this type of cancer was one of the most prevalent cause of death in the US in the age groups of 35-54 and 55-74 year-old women with 1.3%, and 1.5% of all deaths, respectively,

Table 2. The results of *in vitro* cytotoxicity against selected human cancer cell lines (A2780 and A2780R) and healthy (MRC5) cells. IC_{50} values, obtained after 24 h incubation, are given in μM together with the standard deviations, and they are based on triplicate experiments.

Compound	Human cell lines			RF*	SI**
	A2780	A2780R	MRC5		
[Au(iPr)(L1)] (**1**)	7.9±2.4	5.0±1.5	19.8±3.0	0.6	2.5
[Au(iPr)(L2)] (**2**)	9.0±1.4	>25	>25	>2.8	>2.8
[Au(iPr)(L3)] (**3**)	4.4±0.5	7.4±2.2	13.6±1.4	1.7	3.1
[Au(iPr)(L4)] (**4**)	5.0±1.8	7.9±2.4	18.7±1.4	1.6	3.7
[Au(iPr)Cl]	33.6±0.9	>50	>50	>1.5	>1.5
Auranofin	1.5±0.5	3.1±0.2	4.7±0.8	2.1	3.1
Cisplatin (CDDP)	16.8 ± 0.3	>50	>50	>3.0	>3.0

*RF - resistance factor, calculated as the ratio between the IC_{50} value of the resistant cell and sensitive one IC_{50}(A2780R)/IC_{50}(A2780). ** SI– selectivity index expressed as IC_{50}(MRC-5)/IC_{50}(A2780).

With the aim to show the dynamics of the antiproliferative effect of complexes **1–4** against the A2780 cells, time-dependent cytotoxicity experiments (see Table 3) were performed in three incubation times, i.e. 24 h, 48 h and 72 h. The *in vitro* antiproliferative effect of all complexes slightly increases with time. The same trend can be seen also in the case of *Auranofin* and *Cisplatin*. The cytotoxicity of [Au(iPr)Cl] increases only slightly between 24 and 72 h incubation times.

 doi:10.20944/preprints202401.0375.v1

Table 3. The time-dependent *in vitro* cytotoxicity of the labelled compounds against the A2780 cell line.

Compound	24 h	48 h	72 h
[Au(iPr)(L1)] (**1**)	7.9±2.4	3.8±0.5	3.4±0.2
[Au(iPr)(L2)] (**2**)	9.0±1.4	6.6±2.5	5.1±0.7
[Au(iPr)(L3)] (**3**)	4.4±0.5	3.8±1.1	3.0±0.2
[Au(iPr)(L4)] (**4**)	5.0±1.8	4.1±0.8	3.8±0.5
[Au(iPr)Cl]	33.6±0.9	25.7±0.6	26.2±1.5
Auranofin	1.5±0.5	1.0±0.5	0.9±0.4
Cisplatin (CDDP)	16.8 ± 0.3	11.6 ± 3.2	4.4 ± 0.4

2.4. Cellular effects of complex 4 in A2780 cells

The cellular effects of selected complex **4** were tested in human ovarian cancer cells A2780 at a half-cytotoxic concentration of 4.4 μM and an incubation time of 24 h. The flow-cytometry-based assays evaluating the ability of complex **4** to influence the processes of cell cycle progression, induction of cell death by induction of apoptosis/necrosis and/or autophagy, mitochondrial membrane depolarization, and reactive oxygen species (ROS) generation were employed. In these bioassays, complex **4** showed rather weak to no effect on indicated main cellular processes in A2780 cells at a given concentration.

Complex **4** influenced the cell cycle of A2780 cells slightly (see Figure 2A), while only a small decrease in the S phase population was detected in contrast to *Cisplatin*, which arrested most of the cells in S phase and G2/M phase of the cell cycle. In the next step, the induction of cell death by triggering apoptosis/necrosis was evaluated by the Caspase 3/7 green detection reagent/SYTOX AADvanced staining method. Analogously to the previous findings, complex **4** had only a negligible effect on apoptosis/necrosis induction in A2780 cells (see Figure 2B). It caused apoptosis/necrosis in less than 10% of the cells after 24 h of incubation, in sharp contrast to the DNA-binding drug cisplatin, which triggered the apoptosis/necrosis in ca. 40% of cells. These results indicate that the mechanisms associated with antiproliferative effects of tested Au(I) complexes and cisplatin are different. Another cellular process, which indicates the metabolic stress undergoing in the target cells is autophagy. Complex **4** did not show a significant increase in the number of autophagy-positive cells after 24 h incubation (see Figure 2C). A number of processes leading to other types of cell death are associated with impeding of mitochondrial structures and function, e.g. by depleting the mitochondrial membrane potential [22]. Complex **4** slightly increased the number of cells with damaged mitochondrial membranes (see Figure 2D). The molecular basis of mitochondrial membrane destruction is often connected with intracellular overproduction of ROS, but complex **4** was ineffective in this test (see Figure S16).

Based on the presented results, it is likely that complex **4** acts on A2780 cells as an antiproliferative agent and not a cytotoxic one, in contrast to the reference cytotoxic drug cisplatin. Nevertheless, these findings emphasize that there are several other cellular targets and signaling pathways, which can be responsible for the biological activity of the tested Au(I) complexes.

Preprints (www.preprints.org) | NOT PEER-REVIEWED | Posted: 4 January 2024 doi:10.20944/preprints202401.0375.v1

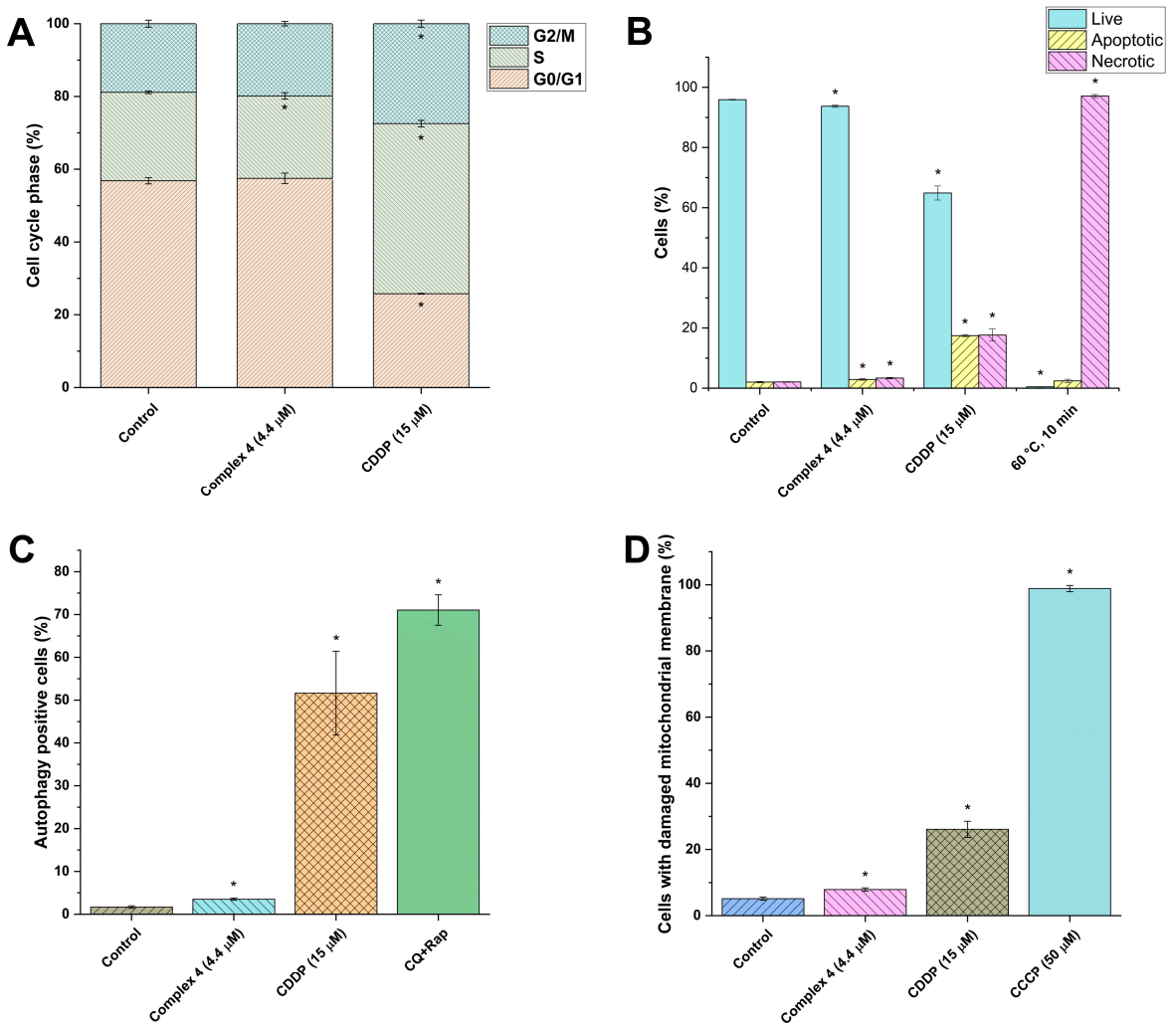

Figure 2. The cellular effects of complex **4** and the reference drug *Cisplatin* on the A2780 cells after 24 h incubation. The effect on cell cycle of A2780 cells (**A**). The effect on the induction of apoptosis/necrosis (B). The effect on the process of autophagy (**C**). The ability of the tested compounds to damage the mitochondrial membrane function (**D**). The statistical significance was considered at the level of * $p<0.05$, with respect to the untreated control group.

2.5. Cell viability and NF-κB activity determination

Before evaluating the anti-inflammatory potential of complexes **1–4**, their highest non-cytotoxic concentration for THP1-Blue™ NF-κB in a serum-free medium had to be determined. The IC_{50} values (concentrations which reduce the cell viability to 50%) were calculated for all the compounds (7.9 ± 1.2 μM for **1**, 10 μM for **2**, 2.2 ± 1.2 μM for **3**, 1.9 ± 1.3 μM for **4**). Based on the obtained data, the concentration of 150 nM was chosen as the highest non-cytotoxic for all the Au(I) complexes.

Pro-inflammatory transcription factor NF-κB, which is activated during inflammation and controls the expression of more than a hundred genes, represent a viable target of gold complexes, including the commercially available drug *Auranofin* [23]. The ability of these complexes to reduce the activity of NF-κB was confirmed by the results given in Figure 3. Complexes **1** and **4** showed comparable effect to *Auranofin* (activity of NF-κB was 87.6% for **1**, 86.7% for **4**, and 84.0% for *Auranofin*), while the overall anti-NF-κB effect of complexes **2** and **3** is lower. These findings are in agreement with contemporary knowledge acquired about the cellular and molecular effects of *Auranofin* [24], which possesses both anticancer features through the inhibition of thioredoxin reductases, moderation of PI3K/Akt pathway, inhibition of STAT3, NF-κB, and PKCiota signalling.

Preprints (www.preprints.org) | NOT PEER-REVIEWED | Posted: 4 January 2024 doi:10.20944/preprints202401.0375.v1

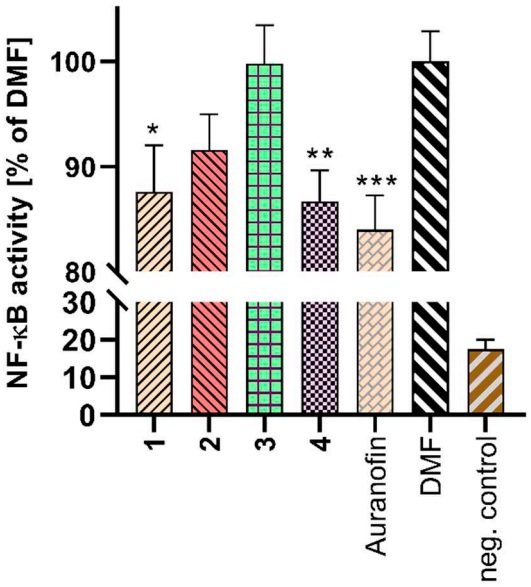

Figure 3. The effect of the tested compounds on NF-κB activity in THP1-Blue™ NF-κB monocytes. Effect of 1 h pre-treatment on LPS-stimulated NF-κB activity detected after 24 h. * $p < 0.05$ compared to the vehicle (DMF), **$p<0.01$ compared to the vehicle (DMF). One-way ANOVA test followed by uncorrected Fisher's LSD analysis was used to express statistical significance. Data are shown as means ± SEM.

2.6. TNF-α detection

The gene expression of pro-inflammatory cytokine TNF-α is under the transcriptional control of NF-κB, however its release into a soluble form can be regulated by several processes [25]. Because complexes showed a moderate effect on the activity of this transcription factor, the analysis of TNF-α production was performed (Figure 4). A statistically significant decrease level of this cytokine was observed for complexes **3** and **4**. The lower amount of TNF-α after the treatment with complex **4** correlates with the lower activity of NF-κB (see Figure 3) caused by complex **4**. Despite a moderate effect on TNF-α production, complex **3** did not significantly influence the NF-κB activity. It may indicate different mechanism of action than direct inhibition of NF-κB.

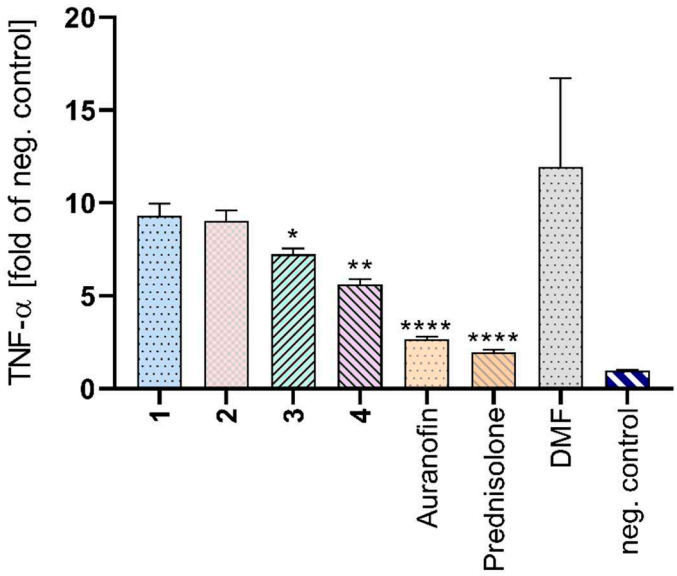

Figure 4. Production of TNF-α in macrophage-like cells *in vitro*. Macrophages delivered from THP1-Blue™ NF-κB cells were pretreated by complexes **1**-**4** (150 nM), *Auranofin* (150 nM), *Prednisolone* (1

μM), or vehicle (0.1 % DMF) only for 1 h. Then, LPS was added, and the level of the secreted cytokine was determined by ELISA technique after 24 h. Graph represents mean ± SEM of three replicates. One-way ANOVA analysis followed by uncorrected Fisher's LSD test was used for statistical evaluation. * Indicates statistical significance ($p < 0.05$) to 0.1% DMF group (vehicle); ** indicates statistical significance ($p < 0.01$) to 0.1% DMF group (vehicle); **** indicates statistical significance ($p < 0.0001$) to 0.1% DMF group (vehicle); neg. control – negative control (without LPS stimulation).

3. Materials and Methods

3.1. General methods used for characterization

The complexes **1–4** were characterized using CHN elemental analyses (CHN analyser Flash Smart CHN, Thermo Scientific), infrared spectroscopy (IR) performed using an ATR technique and in the range of 400-4000 cm^{-1} (Nicolet iS5 FT–IR, Thermo Nicolet), and mass spectrometry (MS) performed using ESI ionization technique in positive/negative modes (Bruker amaZon SL, Bruker). Single crystal X-ray data of complexes **1** and **4** were obtained using a D8 Quest diffractometer (Bruker). Chemicals and solvents were purchased from the commercial sources (Sigma–Aldrich Co., Fluka Co) and were used without any further purification.

3.2. Preparation and characterization of the complexes (1-4)

0.20 mmol of chlorido-[1,3-bis(2,6-diisopropylphenyl)imidazol-2-ylidene]gold(I) was dissolved in dried propan-2-ol (20 mL), and 0.23 mmol of the corresponding HL1–6 ligand and 0.25 mmol of cesium carbonate were added. The reaction mixture was then stirred under a nitrogen atmosphere at 60 °C for 24 h. After that, the reaction mixture was cooled down, and the solid formed by slow evaporation was filtered off and washed with methanol. The products were dried in a vacuum, with yields between 48-95%.

Complex (**1**): Anal. Calcd. for $C_{34}H_{41}N_4FAu$ (Mr = 721,7): C, 56.6; H, 5.7; N, 7.8. Found: C, 56.5; H, 5.5; N, 7.6 %. ESI+MS (methanol, *m/z*): 1201.60 (calcd. 1201.53) $[(Au(iPr))_2(CH_3O)]^+$, 639.29 (calcd. 639.26) $\{[Au(iPr)(CH_3O)]+Na\}^+$, 1255.56 (calcd. 1255.53) $\{[(Au(iPr)(CH_3O))_2]+Na\}^+$, 1305.61 (calcd. 1305.54) $[(Au(iPr))_2(\mu\text{-}L1)]^+$. ESI-MS (methanol, *m/z*): 719.34 (calcd. 719.29) $[Au(iPr)(L1)\text{-}H]^-$, 615.27 (calcd. 615.27) $\{[Au(iPr)(CH_3O)]\text{-}H\}^-$. IR (ATR; cm^{-1}): 417 (w), 453 (m), 472 (m), 500 (m), 551 (w), 619 (w), 634 (w), 702 (vs), 739 (s), 762 (s), 799 (s), 806 (s), 870 (m), 947 (w), 977 (m), 1059 (m), 1127 (s), 1181 (s), 1213 (w), 1261 (m), 1301 (m), 1332 (m), 1360 (w), 1385 (s), 1419 (m), 1467 (s), 1552 (w), 1572 (w), 1592 (w), 2868 (w), 2925 (w), 2955 (m), 2964 (m), 3129 (w), 3157 (w).

Complex (**2**): Anal. Calcd. for $C_{34}H_{41}N_4BrAu$ (Mr = 782,6): C, 52.2; H, 5.3; N, 7.2. Found: C, 52.3; H, 5.1 N, 7.1 %. ESI+MS (methanol, *m/z*): 1201.60 (calcd. 1201.53) $[(Au(iPr))_2(CH_3O)]^+$, 639.29 (calcd. 639.26) $\{[Au(iPr)(CH_3O)]+Na\}^+$, 1255.57 (calcd. 1255.53) $\{[(Au(iPr)(CH_3O))_2]+Na\}^+$, 1367.52 (calcd. 1365.46 for the first isotopic peak) $[(Au(iPr))_2(\mu\text{-}L2)]^+$, 803.25 (calcd. 803.20) $\{[Au(iPr)(L2)]+Na\}^+$, 783.28 (calcd. 781.22 for the first isotopic peak) $\{[Au(iPr)(L2)]\}^+$. IR (ATR; cm^{-1}): 426 (w), 454 (w), 474 (m), 550 (w), 601 (w), 613 (w), 641 (w), 681 (m), 706 (m), 730 (s), 757 (s), 776 (m), 802 (s), 877 (m), 912 (w), 936 (w), 953 (m), 1060 (m), 1103 (w), 1117 (w), 1169 (s), 1186 (w), 1214 (w), 1246 (w), 1291 (m), 1334 (m), 1362 (m), 1386 (s), 1419 (w), 1452 (s), 1466 (s), 1554 (w), 1577 (w), 1594 (w), 2867 (w), 2936 (m), 2960 (m), 3085 (w), 3121 (w), 3149 (w).

Complex (**3**): Anal. Calcd. for $C_{34}H_{41}N_4ClAu$ (Mr = 7381): C, 49.2; H, 5.0; N, 6.8. Found: C, 56.5; H, 5.5; N, 7.6 %. ESI+MS (methanol, *m/z*): 1201.61 (calcd. 1201.53) $[(Au(iPr))_2(CH_3O)]^+$, 639.30 (calcd. 639.26) $\{[Au(iPr)(CH_3O)]+Na\}^+$, 1255.56 (calcd. 1255.53) $\{[(Au(iPr)(CH_3O))_2]+Na\}^+$, 1321.57 (calcd. 1321.52) $[(Au(iPr))_2(\mu\text{-}L3)]^+$, 759.32 (calcd. 759.25) $\{[Au(iPr)(L3)]+Na\}^+$, 737.34 (calcd. 737.27) $\{[Au(iPr)(L3)]\}^+$. IR (ATR; cm^{-1}): 418 (w), 454 (w), 538 (m), 550 (m), 567 (w), 591 (w), 642 (w), 707 (m), 760 (vs), 773 (s), 787 (s), 803 (s), 924 (w), 935 (w), 947 (w), 1010 (s), 1034 (w), 1115 (w), 1159 (w), 1205 (w), 1271 (m), 1300 (m), 1326 (m), 1344 (w), 1362 (w), 1384 (m), 1401 (s), 1419 (w), 1469 (s), 1548 (w), 1593 (m), 2868 (w), 2929 (w), 2961 (m), 3032 (w), 3079 (w), 3121 (w), 3149 (w).

 doi:10.20944/preprints202401.0375.v1

Complex (**4**): Anal. Calcd. for $C_{34}H_{41}N_4IAu$ (Mr = 829,6): C, 55.3; H, 5.6; N, 7.6. Found: C, 55.6; H, 5.5; N, 7.5 %. ESI+MS (methanol, *m*/*z*): 1201.60 (calcd. 1201.53) $[(Au(iPr))_2(CH_3O)]^+$, 639.30 (calcd. 639.26) $\{[Au(iPr)(CH_3O)]+Na\}^+$, 1255.56 (calcd. 1255.53) $\{[(Au(iPr)(CH_3O))_2]+Na\}^+$, 1413.49 (calcd. 1413.45) $[(Au(iPr))_2(\mu\text{-}L4)]^+$, 829.25 (calcd. 829.20) $\{[Au(iPr)(L4)]\}^+$, 851.23 (calcd. 851.19) $\{[Au(iPr)(L4)]+Na\}^+$. IR (ATR; cm^{-1}): 417 (w), 430 (w), 455 (w), 472 (w), 517 (m), 551 (w), 574 (w), 588 (m), 670 (w), 707 (m), 766 (s), 786 (s), 804 (m), 854 (m), 919 (w), 983 (w), 1035 (w), 1060 (w), 1110 (w), 1159 (w), 1184 (w), 1201 (w), 1237 (w), 1267 (w), 1292 (m), 1318 (m), 1364 (w), 1392 (s), 1416 (m), 1466 (s), 1488 (w), 1542 (w), 1552 (w), 1589 (m), 2866 (w), 2925 (w), 2955 (m), 2962 (w), 3029 (w), 3080 (w), 3115 (w), 3145 (w).

3.3. Single-crystal X-ray diffraction analysis

Single crystals of complexes **1** and **4** suitable for single-crystal X-ray analysis were prepared by slow evaporation from propan-2-ol/methanol (1:1) solutions. The data were collected on a Bruker D8 QUEST diffractometer equipped with a PHOTON 100 CMOS detector. K. The APEX3 software package [26] was used for data collection and reduction. The molecular structure was solved by direct methods (SHELXS) and refined by full-matrix least-squares procedure SHELXL [27]. Hydrogen atoms were found in the difference Fourier maps and refined using a rigid model, with C–H = 0.95 Å $(CH)_{ar}$ and (CH), and C–H = 0.98 Å (CH_3), and with $U_{iso}(H) = 1.2U_{eq}(CH)$ and $U_{iso}(H) = 1.5U_{eq}(CH_3)$. The figures were drawn, and additional structural calculations were performed, using DIAMOND [28] and MERCURY [29] software. Owing to highly disordered unknown solvent molecule(s), a region of disordered electron density was treated using a SQUEEZE procedure [30] incorporated in PLATON software [31]. The crystal data and structure refinement details are given in Table 4.

Table 4. Crystal data and structure refinement for [Au(iPr)(L1)] (**1**) and [Au(iPr)(L4)] (**4**).

Empirical formula	$C_{34}H_{41}N_4FAu$	$C_{34}H_{41}N_4IAu$
Formula weight	720.66	828.56
Temperature	293(2) K	150(2) K
Wavelength	0.71073 Å	0.71073 Å
Crystal system	Triclinic	Triclinic
Space group	P-1	P-1
Unit cell dimensions	a = 10.812(4) Å, α = 87.641(15)°	a = 9.563(4) Å, α = 81.364(16)°
	b = 11.617(5) Å, β = 77.852(13)°	b = 11.986(5) Å, β = 87.163(14)°
	c = 14.396(5) Å, γ = 66.83(2)°	c = 16.130(7) Å, γ = 77.766(18)°
Volume	1623.4(11) $Å^3$	1786.0(12) $Å^3$
Z	2	2
Density (calculated)	1.474 g/cm^3	1.541 g/cm^3
Absorption coefficient	4.564 mm^{-1}	5.008 mm^{-1}
F(000)	720	808
Crystal size	0.260 x 0.240 x 0.200 mm	0.160 x 0.120 x 0.100 mm
θ range for data collection	1.909 to 24.999°.	2.180 to 25.000°.
Index ranges	$-12 \le h \le 12$, $-13 \le k \le 13$, $-17 \le l \le 17$	$-11 \le h \le 11$, $-14 \le k \le 14$, $-19 \le l \le 19$
Reflections collected	29392	37929
Independent reflections	5713 [*R*(int) = 0.0666]	6293 [*R*(int) = 0.0481]
Completeness to θ = 25.0°	100.0 %	99.9 %
Absorption correction	Semi-empirical from equivalents	Semi-empirical from equivalents
Refinement method	Full-matrix least-squares on F^2	Full-matrix least-squares on F^2
Data / restraints / parameters	5713 / 0 / 369	6293 / 0 / 369
Goodness-of-fit on F^2	1.086	1.053
Final *R* indices [$I>2\sigma(I)$]	*R*1 = 0.0312, *w*R2 = 0.0680	*R*1 = 0.0195, *w*R2 = 0.0393
R indices (all data)	*R*1 = 0.0465, *w*R2 = 0.0715	*R*1 = 0.0263, *w*R2 = 0.0406

 doi:10.20944/preprints202401.0375.v1

3.4. In vitro cytotoxicity against human ovarian cancerous (A2780 and A2780R) and normal (MRC-5) cell lines

The *in vitro* cytotoxicity of complexes (**1–4**), and [Au(PPh$_3$)Cl], *Auranofin* and *Cisplatin*, for comparative purposes, was determined by the MTT assay at various time of incubation (24, 48 and 72 h) as more detailed described previously [17–20]. The testing was performed on the ovarian carcinoma (A2780), *Cisplatin*-resistant ovarian carcinoma (A2780R) human cell lines which were obtained from ATCC collection of cell lines and cultivated according to producer's instructions. The reference normal cell line of human foetal fibroblasts (MRC-5) was obtained from the same commercial source and maintained according to the producer's instructions. The half-maximal inhibitory concentrations (IC_{50}) were calculated from dose-response curves by means of the GraphPad Prism 6 software (GraphPad Software, San Diego, USA).

3.5. Cell cycle analysis in A2780

The A2780 cells were cultured in RPMI-1640 (Sigma-Aldrich Co., Burlington, MA, USA) medium containing 10% FBS and then 10,000 cells were seeded per well in a 96-well plate. The cells were incubated for 24 hours at 37°C in a 5% CO_2 atmosphere. The representative complex **4** was then added to the cells to a final concentration of 4.4 μM by diluting its 4.4 mM stock solution in DMF into the cell culture medium, and the cells were incubated for an additional 24 hours. The cells incubated with 0.1% DMF in cell medium served as a negative control. After the incubation period, cells were washed with PBS and processed according to the instructions of the BD Cycletest™ Plus DNA Reagent Kit (Becton Dickinson, Franklin Lakes, NJ, USA). The resulting samples were analyzed using a BD FACSVerse flow cytometer (Becton Dickinson, USA). Three independent measurements were performed, each done in triplicate.

3.6. Cell death induction in A2780

Induction of cell death was analyzed using CellEvent™ Caspase-3/7 Green Flow Cytometry Assay Kit in combination with SYTOX AADvanced dead cell stain (Thermo Fisher Scientific, USA). The procedure was done as follows: The A2780 cells were cultured in RPMI-1640 medium (Sigma-Aldrich Co.) containing 10% FBS and then 50,000 cells were seeded per well in a 24-well plate. The cells were incubated for 24 hours at 37 °C in a 5% CO_2 atmosphere. Complex **4** was then added to the cells to a final concentration of 4.4 μM by diluting its 4.4 mM stock solution in DMF into the cell culture medium, and the cells were incubated for an additional 24 hours. Cells incubated with 0.1% DMF in cell medium served as a negative control. After the incubation period, the cell medium was aspirated and saved, cells were washed with PBS and trypsinized using 0.25% Trypsin-EDTA (Gibco™, Waltham, MA, USA). After cell detachment, trypsin was stopped by the addition of complete cell medium and the obtained fractions were pooled to collect all cells including floating dead cells contained in the original cell medium and PBS wash. To the resulting cell suspensions, 1 μl CellEvent™ Caspase 3/7 Green Detection Reagent per 1 ml sample was added and the samples were incubated for 25 minutes in the dark at 37 °C. After 25 minutes, 1 μl of SYTOX AADvanced dead cell stain per 1 ml of sample was added to the cell suspensions and the samples were incubated for 5 minutes in the dark at 37 °C. The samples were then analyzed using a BD FACSVerse flow cytometer (Becton Dickinson, USA). Three independent measurements were performed, each done in duplicate.

3.7. Autophagy induction in A2780

To detect autophagy induction upon exposure to complex **4**, A2780 cells were cultured in RPMI-1640 medium (Sigma-Aldrich Co.) containing 10% FBS and then 50,000 cells were seeded per well in a 24-well plate. The cells were incubated for 24 hours at 37°C in a 5% CO_2 atmosphere. Complex **4** was then added to the cells to a final concentration of 4.4 μM by diluting its 4.4 mM stock solution in DMF into the cell culture medium, and the cells were incubated for an additional 24 hours. Cells incubated with 0.1% DMF in cell medium served as a negative control. For positive control, cells were

 doi:10.20944/preprints202401.0375.v1

incubated with the addition of 15 μM chloroquine and 0.5 μM rapamycin for 24 hours. Cells were then rinsed with PBS and trypsinized with 0.25% Trypsin-EDTA (Gibco™). Trypsin was stopped by the addition of a complete cell medium, and CYTO-ID® Green Detection Reagent dye was added to the resulting cell suspensions according to the CYTO-ID® Autophagy detection kit manual (Enzo Life Sciences, US). After staining, the cells were analyzed using a BD FACSVerse flow cytometer (Becton Dickinson, USA). Three independent measurements were performed, each done in duplicate.

3.8. ROS and superoxide detection

To assess the generation of total ROS (Reactive Oxygen Species) and superoxide in A2780 cells after exposure to the tested compounds, we employed the ROS-ID® Total ROS/Superoxide detection kit (Enzo Life Sciences, USA). The A2780 cells were cultured in RPMI-1640 (Sigma-Aldrich Co.) medium containing 10% FBS and then 10,000 cells were seeded per well in a 96-well plate. The cells were incubated for 24 hours at 37 °C in a 5% CO_2 atmosphere. Complex **4** was then added to the cells to a final concentration of 4.4 μM by diluting its 4.4 mM stock solution in DMF into the cell culture medium, and the cells were incubated for an additional 24 hours. Cells incubated with 0.1% DMF in cell medium served as a negative control. After incubation, cells were washed with 1× ROS wash buffer and then fluorescent probes for ROS and Superoxide detection were added to the cells according to the kit manufacturer's instructions. All test conditions were prepared simultaneously with the addition of probes in the presence and absence of the ROS/Superoxide inducer pyocyanin at a concentration of 500 μM. Subsequently, the samples were incubated for 40 min and analyzed using a fluorescence microplate reader (Infinite M200Pro, Tecan, Switzerland). Three independent measurements were performed, each done in triplicate.

3.9. Mitochondrial membrane potential analysis

Detection of mitochondrial membrane potential (MPP) was performed using the MITO-ID® Membrane potential detection kit (Enzo Life Sciences, USA). The procedure was as follows: The A2780 cells were cultured in RPMI-1640 medium (Sigma-Aldrich Co.) containing 10% FBS and then 50,000 cells were seeded per well in a 24-well plate. The cells were incubated for 24 hours at 37°C in a 5% CO_2 atmosphere. The representative complex **4** was then added to the cells to a final concentration of 4.4 μM by diluting its 4.4 mM stock solution in DMF into the cell culture medium, and the cells were incubated for an additional 24 hours. Cells incubated with 0.1% DMF in cell medium served as a negative control. Cells that had been incubated at 37 °C for 5 min before staining with 50 μM *N*-(4-chlorophenyl)carbonohydrazonoyl dicyanide (CCCP) were used as a positive control. After the incubation period, the cell medium was aspirated and saved, cells were washed with PBS and trypsinized using 0.25% Trypsin-EDTA (Gibco™). After cell detachment, trypsin was stopped by the addition of complete cell medium and the obtained fractions were pooled to collect all cells including floating cells contained in the original cell medium and PBS wash. The cells were then centrifuged for 5 min at 200×g and at RT. The supernatants were discarded, and the cell pellets were re-suspended in a staining solution that was prepared according to the kit manufacturer's instructions. After staining, cells were analyzed using a BD FACSVerse flow cytometer (Becton Dickinson, USA). Three independent measurements were performed, each done in duplicate.

3.10. Descriptive statistics evaluation

The descriptive statistics evaluation of the obtained results was performed using Statistica software ver. 14.0.0.15 (TIBCO Software Inc.). To assess the significance of the difference between two values, an independent group t-test was performed. Differences were evaluated at a significance level of $p<0.05$ (*). Test conditions were always compared relative to the negative control sample.

3.11. Cell maintenance and viability determination

THP1-Blue™ NF-κB cell line (InvivoGen; San Diego, CA, USA) was used to evaluate anti-NF-κB activity of complexes **1–4** and reference drugs *Auranofin* and *Prednisolone*. The cells were cultivated

 doi:10.20944/preprints202401.0375.v1

in RPMI (Roswell Park Memorial Institute) 1640 medium (Biosera; Nuaille, France) supplemented with 10% foetal bovine serum (FBS) and antibiotics (100 U/mL penicillin and 100 mg/mL streptomycin) (both from Merck), and antimicrobial reagent Normocin™ (InviGen). All subsequent experiments were performed in serum-free medium. For further experiments, the non-toxic concentrations for the tested compounds dissolved in DMF were used. Such concentrations were determined using a Cell Counting Kit-8 (CCK-8; Merck) according to the manufacturer's instructions after 24 h incubation in serum-free medium.

3.12. NF-κB activity determination

A model of lipopolysaccharide (LPS) challenged THP1-Blue™ NF-κB cells was used to evaluate the ability of complexes **1–4** and reference drugs *Auranofin* and *Prednisolone* dissolved in DMF at non-toxic concentrations (all 150 nM, and prednisolone 1 μM) to influence the function of transcription factor. The cells were pre-treated by the tested compounds. After 1 h, LPS from *E. coli* (Merck) dissolved in serum-free RPMI 1640 medium (500 ng/mL) was added. After 24 h incubation, the activity of NF-κB was determined as amount of secreted embryonic alkaline phosphatase using Quanti-Blue™ medium (InvivoGen).

3.13. TNF-α release detection

THP1-Blue™ NF-κB cells were treated by complexes **1–4**, reference drugs, and LPS in the same way as in the case of NF-κB assay (see above). After 24 h incubation, the amount of produced TNF-α in cultivation medium was determined by ProQuantum Human TNFa Immunoasay Kit (Invitrogen) according to manufacturer's instructions.

4. Conclusions

Four gold(I)-NHC complexes **1–4** containing 7-azaindole derivatives were prepared, characterized, and evaluated for their *in vitro* anticancer (on ovarian A2780 and *Cisplatin*-resistant A2780R cells) and anti-inflammatory effects (pro-inflammatory transcription factor NF-κB, and tumour necrosis factor TNF-α). All the complexes revealed considerable antiproliferative effects on the cancer cells (with $IC_{50} \approx 4–9$ μM), except for **2** on A2780R with $IC_{50} > 25$ μM, showing significantly higher cytotoxicity than anticancer drug *Cisplatin*. In addition to that, they also revealed a relatively good selectivity over healthy cells (MRC-5), with the values of selectivity index, SI > 2.5. The cellular effects of selected complex **4** were tested on A2780 cells by means of several flow-cytometry based assays (cell cycle modification, apoptosis/necrosis and autophagy induction, intracellular ROS generation, and mitochondrial membrane destruction). Yet no significant effects on these major cellular processes were detected after the 24 h incubation. In addition to these methods, the ability of complexes **1–4** to influence the inflammation in LPS-activated macrophages, was evaluated. Complexes **1** and **4** revealed the ability to reduce the activity of NF-κB, while complex **4** significantly reduced the level of excreted soluble TNF-α.

Supplementary Materials: The following supporting information can be downloaded at the website of this paper posted on Preprints.org, Figures **S1–S4** ESI-MS spectra of complexes [Au(iPr)(HLn)] 1–4 measured in MeOH solution in positive/negative ionization modes; Figures **S5–S8** IR spectra of complexes [Au(iPr)(HLn)] 1–4; Figures **S9–S12** IR spectra of free HL1-4 ligands; Figure **S13** IR spectrum of the starting [Au(iPr)Cl] complex; Figure **S14** Part of crystal structure of complex 1, showing the C–H...N and C–H...C non-covalent contacts (blue dotted lines) connecting individual molecules of 1 into infinite 1D-polymeric chains; Figure **S15** Part of crystal structure of complex 4, showing the C–H...N, C–H...C and C...C non-covalent contacts (blue dotted lines) connecting two individual molecules of 4 into centrosymmetric dimmers. The presence of voids associated with the squeezed atoms belonging to the unknown solvent molecule(s) are shown in yellow color; Figure **S16** The intracellular levels of ROS (A) and superoxide (B) in A2780 cells after 24 h incubation with half-cytotoxic concentrations of (4), and reference drug *Cisplatin*.

Author Contributions: Conceptualization, Z.T. and J.V.; methodology, Z.T., J.V., J.B., J.H. and Z.D.; validation, Z.T., J.V., J.B., M.Č. J.H. and Z.D; investigation Z.T., J.V., J.B., M.Č. and Z.D,.; resources, Z.T.; writing—original draft preparation, Z.T., J.V.; writing—review and editing, Z.T., J.V., J.B., M.Č., J.H. and Z.D.; visualization, Z.T.,

J.V., J.B., M.Č. and J.H.; supervision, Z.T.; project administration, Z.T.; funding acquisition, Z.T.. All authors have read and agreed to the published version of the manuscript.

Funding: This research was funded by the Czech Sciences Foundation, a grant number CSF Bilateral AT-CZ 21-38204L (Z.T.).

Data Availability Statement: Cambridge Crystallographic Database contains the supplementary crystallographic data for the [Au(iPr(L1)] (**1**) and the [Au(iPr(L4)] (**4**) , CCDC deposition numbers are as follows: 2315302, and 2315303, respectively. These data can be obtained free of charge via www.ccdc.cam.ac.uk/conts/retrieving.html (or from the Cambridge Crystallographic Data Centre, 12 Union Road, Cambridge CB21EZ, UK; fax: (+44) 1223-336-033; or de-posit@ccdc.cam.ac.uk). Supplementary materials to this article can be found online at doi:

Acknowledgments: The authors thank Renata Jakubcová for FTIR spectra measurements, Marta Rešová for *in vitro* cytotoxicity testing, and Josef Mašek for help with confocal microscopy experiments.

Conflicts of Interest: The authors declare no conflict of interest.

References

1. Marion, N., Nolan, S. P.. N-Heterocyclic carbenes in gold catalysis. *Chem. Soc. Rev*., **2008**, 37, 1776–1782. https://doi.org/10.1039/B711132K
2. Scott, S. C.; Cadge, J. A.; Bower, J. F.; Russell, Ch. A. A Hemilabile NHC-Gold Complex and its Application to the Redox Neutral 1,2-Oxyarylation of Feedstock Alkenesl. *Angew. Chem. Int. Ed*. **2023**, 62, e202301526, https://doi.org/10.1002/anie.202301526
3. Mora, M.; Gimeno, M. C.; Visbal, R. Recent advances in gold–NHC complexes with biological properties. *Chem. Soc. Rev*., **2019**, 48, 447—462, https://doi.org/10.1039/c8cs00570b
4. Goetzfried, S. K.; Kapitza, P.; Gallati, Ch. M.; Nindl, A.; Cziferszky, M.; Hermann, M.; Kircher, B.; Gust R. Investigations of the reactivity, stability and biological activity of halido (NHC)gold(I) complexes. *Dalton Trans*., **2022**, 51, 1395–1406, https://doi.org/10.1039/d1dt03528b
5. Bertrand, B.; Casini, A. A golden future in medicinal inorganic chemistry: the promise of anticancer gold organometallic compounds. *Dalton Trans*., **2014**, 43, 4209–4219, https://doi.org/10.1039/c3dt52524d
6. Hussaini, S. Y.; Haque, R. A.; Razali, M. R. Recent progress in silver(I)-, gold(I)/(III)- and palladium(II)-N-heterocyclic carbene complexes: A review towards biological perspectives. *J. Organomet. Chem*., **2019**, 882, 96e111, https://doi.org/10.1016/j.jorganchem.2019.01.003
7. Augello, G.; Azzolina, A.; Rossi, F.; Prencipe, F.; Mangiatordi, G. F.; Saviano, M.; Ronga, L.; Cervello, M.; Tesauro, D. New Insights into the Behaviour of NHC-Gold Complexes in Cancer Cells. *Pharmaceutics* **2023**, 15, 466, https://doi.org/10.3390/pharmaceutics15020466
8. König, P.; Zhulenko, R.; Suparman, E.; Hoffmeister, H.; Bückreiß.; Ott, I.; Bandas, G. A biscarbene gold(I)-NHC-complex overcomes cisplatin-resistance in A2780 and W1 ovarian cancer cells highlighting pERK as regulator of apoptosis. *Cancer Chemotherapy and Pharmacology*, **2023**, 92, 57–69. https://doi.org/10.1007/s00280-023-04548-1,
9. Massai, L. R.; Messori, L.; Carpentieri, A.; Amoresano, A.; Melchiorre, Ch.; Fiaschi, T.; Modesti, A.; Gamberi, T.; Magherini, F. The effects of two gold-N-heterocyclic carbene (NHC) complexes in ovarian cancer cells: a redox proteomic study. *Cancer Chemotherapy and Pharmacology*. **2022,** 89, 809–823. https://doi.org/10.1007/s00280-022-04438-y
10. Serebryanskaya, T. V.; Zolotarev, A. A.; Ott, I. A novel aminotriazole-based NHC complex for the design of gold(i) anti-cancer agents: synthesis and biological evaluation. *Med. Chem. Commun*., **2015**, 6, 1186–1189, https://doi.org/10.1039/c5md00185d
11. Scattolin, T.; Lippmann, P.; Beliš, M.; van Hecke, K.; Ott, I.; Nolan, S. P. A simple synthetic entryway into (N-heterocyclic carbene)gold-steroidyl complexes and their anticancer activity. *Appl. Organomet. Chem*. **2022**, e6624, https://doi.org/10.1002/aoc.6624
12. Filho, M. S.; Scatollin, T., Dao, P.; Tzouras, N. V.; Benhida, R.; Saab, M.; van Hecke, K.; Lippman, P.; *et al*., Straightforward synthetic route to gold(i)-thiolato glycoconjugate complexes bearing NHC ligands (NHC = N-heterocyclic carbene) and their promising anticancer activity. *New J. Chem*., **2021**, 45, 9995–10001, https://doi.org/10.1039/d1nj02117f
13. Ott, I. Chapter Four - Metal *N*-heterocyclic carbene complexes in medicinal chemistry. *Advances in Inorganic Chemistry*, **2020** 75, 121-148, https://doi.org/10.1016/bs.adioch.2019.10.008
14. Shen, S.; Shen, J.; Wang, F.; Min, J. Molecular mechanisms and clinical implications of the gold drug auranofin. *Coord. Chem. Rev.* **2023**, 493, 215323, https://doi.org/10.1016/j.ccr.2023.215323
15. Hatem, E.; Banna, N. E.; Heneman-Masurel, A.; Baile, D.; Vernis, E.; Riquier, S.; Colinelli-Cohen, M.; Guittet, O.; *et al. Cancers* **2022**, 14(19), 4864; https://doi.org/10.3390/cancers14194864

16. Liu, Y.; Lu, Y.; Xu, Z.; Ma, X.; Chen, X.; Liu, W. Repurposing of the gold drug auranofin and a review of its derivatives as antibacterial therapeutics. *Drug Discovery Today*, **2022**, 27(7), 1964-1973, https://doi.org/10.1016/j.drudis.2022.02.010
17. Trávníček, Z.; Vančo, J.; Čajan, M.; Belza, J.; Popa, I.; Hošek, J., Lenobel, R.; Dvořák, Z. Gold(I) N-heterocyclic carbene (NHC) complexes containing 6-mercaptopurine derivatives and their in vitro anticancer and anti-inflammatory effects. *Appl. Organomet. Che*m., **2023**, under review.
18. Štarha, P.; Trávníček, Z.; Crlíková, Z.; Vančo, J.; Kašpárková, J.; Dvořák, Z. Half-Sandwich Ir(III) Complex of N1-Pyridyl-7-azaindole Exceeds Cytotoxicity of Cisplatin at Various Human Cancer Cells and 3D Multicellular Tumor Spheroids. *Organometallics*. **2018**, 37, 2749-2759. https://doi.org/10.1021/acs.organomet.8b00415
19. Štarha, P.; Hošek, J.; Dvořák, Z.; Suchý, P.; Popa, I.; Pražanová, G.; Trávníček, Z. Pharmacological and Molecular Effects of Platinum(II) Complexes Involving 7-Azaindole Derivatives. *PLoS ONE*, **2014**, 9(3): e90341. https://doi.org/10.1371/journal.pone.0090341
20. Z. Trávníček, J. Vančo, Z. Dvořák, N-heterocyclic carbene complexes of gold with bicyclic N-donor ligands and using these complexes to prepare antitumor therapy medicaments, Czech Patent no. 307954, granted 31.07.2019, https://isdv.upv.cz/webapp/resdb.print_detail.det?pspis=PT/2018-87&plang=CS
21. Pouchert, C.J. The Aldrich Library of Infrared Spectra, 3rd ed., Aldrich Chemical Company Press: Milwaukee, USA, **1981**; pp. 1-1850
22. Lemasters, J. J.; Qian, T.; Bradham, C. A.; Brenner, D. A.; Cascio, W. E.; Trost, L. C.; Nishimura, Y.; Niemine, A.-L.; Herman, B. Mitochondrial Dysfunction in the Pathogenesis of Necrotic and Apoptotic Cell Death. *J Bioenerg Biomembr.*, **1999**, 305–319. https://doi.org/10.1023/A:1005419617371
23. Berners-Price, S.J.; Filipovska, A. Gold compounds as therapeutic agents for human diseases. *Metallomics* **2011**, *3*, 863–873. https://doi.org/10.1039/c1mt00062d
24. Gamberi, T.; Chiappetta, G.; Fiaschi, T.; Modesti, A.; Sorbi, F.; Magherini. F. Upgrade of an old drug: Auranofin in innovative cancer therapies to overcome drug resistance and to in-crease drug effectiveness. *Med Res Rev*., **2022** 42(3), 1111-1146. https://doi.org/10.1002/med.21872
25. Kalliolias, G. D.; Ivashkiv, L. B.; TNF biology, pathogenic mechanisms and emerging therapeutic strategies. Nat. Rev. Rheumatol. **2016**, 12(1), 49-62. https://doi.org/10.1038/nrrheum.2015.169
26. APEX3 Software Suite, © **2016** Bruker AXS Inc., 5465 East Cheryl Parkway, Madison, WI 53711.
27. Sheldrick, G. SHELXT - Integrated space-group and crystal-structure determination. *Acta Crystallogr. A* **2015**, *71*, 3-8. https://doi.org/10.1107/S2053273314026370
28. Diamond - Crystal and Molecular Structure Visualization, **2021**, Crystal Impact - Dr. H. Putz & Dr. K. Brandenburg GbR, Kreuzherrenstr. 102, 53227 Bonn, Germany.
29. Macrae, C.F.; Bruno, I.J.; Chisholm, J.A.; Edgington, P.R.; McCabe, P.; Pidcock, E.; Rodriguez-Monge, L.; Taylor, R.; van de Streek, J.; Wood, P.A. Mercury CSD 2.0 - new features for the visualization and investigation of crystal structures. *J. Appl. Crystallography* **2008**, *41*, 466-470. https://doi.org/10.1107/S0021889807067908
30. Spek, A.L. PLATON SQUEEZE: a tool for the calculation of the disordered solvent contribution to the calculated structure factors. *Acta Cryst.* **2015,** *C71*, 9–18. https://doi.org/10.1107/S2053229614024929
31. Spek, A.L. Single-crystal structure validation with the program PLATON. *J. Appl. Crystallogr.* **2003**, *36*, 7-13. https://doi.org/10.1107/S0021889802022112。